A complex 3D volume for sub-basalt imaging

F. Martini[1], R.W. Hobbs[2] C.J. Bean[1] and R. Single[3]

Thick successions of basalt and basaltic-andesite lavas flows were extruded during continental break-up and they cover pre-existing sedimentary basins often of interest for hydrocarbon exploration. With conventional seismic acquisition and processing methods, it is difficult to image both the internal architecture of the volcanic succession as well as the underlying sub-basalt structure. The use of synthetic data can help us to understand the poor sub-basalt imaging quality and to develop effective acquisition and processing approaches useful for real data. Moreover, non-seismic methods have been successful in improving understanding of overall geometries of sub-basalt targets. Therefore, integration of seismic and non-seismic data seems to yield promising results and needs to be explored further. From all these considerations, the necessity of a realistic 3D basalt model that would allow simulating realistic seismic and non-seismic data, on one hand to test seismic acquisition and processing techniques, and on the other to develop strategies for geophysical data integration into a common methodology to overcome the sub-basalt imaging problem. A complex 3D model was built adapting all the information available from interpretation of seismic data, log data, gravity data, and geological observation. Seismic and non-seismic synthetic data have been produced on the model. In this paper we present the methodology to develop the 3D model as well as the initial results from data simulations. The model and the data are available to the public, through the authors of the present paper.

Introduction

The problem of seismic imaging through basalt is particularly acute in many areas where potential hydrocarbon bearing structures are overlain by basaltic sequences of stacked flows up to several kilometres thick (e.g., the North Atlantic, west African and Brazilian margins). In these areas, thick successions of basalt and basaltic-andesite lavas flows were extruded during continental break-up (i.e. 'flood basalts') and they cover pre-existing sedimentary basins, that may be of interest for hydrocarbon exploration. With conventional seismic acquisition and processing methods, it is difficult to image both the internal architecture of the volcanic succession as well as the underlying sub-basalt structure. The imaging problem is due to a combination of factors; both the heterogeneous nature of basalt flow interfaces and their internal structure have strong affects (Fliedner and White, 2001, Martini and Bean, 2002a, Martini and Bean, 2002b, Martini et al., submitted.). The role of wave scattering in seismic imagery is well documented in the literature (Gibson and Lavender, 1988, Pullammanappallil et al., 1997, Martini et al., 2001) as well as the effects of irregular interfaces on wave propagation (Paul and Campillo, 1988, Purnell et al., 1990, Ruud and Hestholm, 2000, Hestholmn and Ruud, 2000, Martini and Bean, 2002a, Martini and Bean, 2002b, Ziolkowski et al., 2003).

Intra-lava flow velocity variations, caused by compositional and structural variability within the individual flows (low velocity at the top and base versus high velocity in the massive core), combined with inter-layering between lava flows, sediments, tuff, sills, and hyaloclastites, contribute to the heterogeneous internal structure of the volcanic succession. This complex 3D structure attenuates, scatters and multiply reflects the energy that gets transmitted into the basalt layers through the high impedance contrast at the top of the flows. Also, top and base basalt are not flat regular surfaces, but often have a complex topography, which compounds the disruptive effect on wave propagation. All these factors combine to substantially reduce the quality of sub-basalt seismic imaging.

The use of synthetic data can help us to understand the influence of these factors on sub-basalt images, and to explore effective acquisition and processing approaches useful for real data. For seismic data in basalts, 3D wave propagation in a 3D model is required to obtain synthetic data that are quantitatively similar to the 3D real world (Martini et al., submitted). Hence the necessity for a realistic 3D basalt model.

Non-seismic methods have been successful in improving understanding of overall geometry for sub-basalt targets, e.g., electric and electromagmatic methods (e.g., Manglik and Verma, 1998, Warren and Srnka, 1992, MacGregor et al., 1999, MacGregor and Sinha, 2002, Jegen et al., 2002), gravity (e.g., Murphy at al., 2002), compliance methods (e.g., Crawford, 2002). Integration of seismic and non-seismic data has been tested for some of the methods and has yielded promising results (Manglik and Verma, 1998; Hautot et al., 2002). However, these methods cannot produce the clarity of image required for conventional risk assessment for hydrocarbon exploration.

[1] *Seismology and Computational Rock Physics Lab., Geophysics Group, Dept. of Geology, University College Dublin, Belfield, Dublin 4.*
[2] *Department of Earth Science, University of Durham, UK.*
[3] *Department of Earth Science, University of Durham, UK, now at: Heidrun PETEK, Statoil A.S.A., P.O.Box 273, N-7501, Stjørdal, Norway.*

© 2005 EAGE

The aim of this work was to create a realistic 3D velocity model that would help, through synthetic wave simulations, in providing an overall assessment of the sub-basalt imaging issue. This model was designed, based on information extracted from real data, to replicate the velocity distribution, the highly scattering internal basalt structure, and the irregular flow interfaces. The model was created and parameterised such that it is possible to simulate data with different techniques (i.e. seismic, gravity, magnetic, EM) and, therefore, offers an opportunity to develop strategies based on data integration into a common methodology for sub-basalt exploration.

In this paper we present the methodology used to develop the 3D model, as well as the initial results from data simulations. Both model and seismic data are available to the public to be downloaded and used for testing new processing techniques. We offer the model as a representation of the basalt equivalent of the SEG/EAGE salt and Marmousi model (i.e. Aminzadeh et al., 1997, Versteeg, 1994).

Model construction

In order to reproduce synthetic data comparable to real data, the 3D model has to match the features of the real world geology as closely as reasonably possible. This information is included deterministically when possible, and statistically when the deterministic knowledge of those features is not available. Therefore, to overcome the lack of deterministic knowledge of small-scale heterogeneity, our model incorporates large-scale observations from seismic data and geological mapping, and the small scale statistical information extracted from seismic data and geological mapping, and also borehole data.

A specific seismic dataset was chosen as a base for our model, so we could ensure our synthetic data would closely resemble the field data. The model features main basalt and pre- and post-basalt interfaces derived and adapted from those seismic reflection data. The basalt thickness is a 'lava cake' structure, in which the basalt flows have thicknesses derived from observation of outcrops in the field (Jerram, 2002, Single and Jerram, 2004). The individual flows are created using statistical velocity information taken from the analysis of borehole sonic and density logs. The rest of the model (pre- and post-basalt sediment layers, sills, basement) has been filled according to the geological model derived from the seismic field data and to match potential field data.

Original data

The geological model was constructed on interpreted seismic data from the GFA-99 survey acquired by WesternGeco in the Faeroe-Shetland basin. The survey consists of a coarse grid of 2D lines (Figure 1a), with a total length of 1700 km. The data were recorded using a single boat towing an 11.4 km long streamer with a 25 m shot interval, and a total record length of 10 sec (Bagaini et al., 2000). The data were processed by Geco-Prakla and, for the purposes of this project, interpreted at the University of Durham. Six 2D seismic lines at 90° from each other with nine seismic crossovers were interpreted at a node spacing of 500 m along the profiles. Interpolation across the dataset performed in GoCad on this interpretation produced a set of surfaces over a 50 km x 50 km area. These surfaces, which provided the starting point for the 3D model, are shown in Figure 1b. Gravity modelling and inversion were also performed on these data in an effort to estimate the basement depth and geometry.

Interfaces

Re-gridding and re-sampling

The surfaces interpreted from the seismic and interpolated in GoCad were provided in form of x, y and z (depth) coordinates on an irregularly spaced grid with a nominal node spacing of 500 m (Figure 2a). The irregular spacing is due to the nature of the interpolation process in Gocad, which does not work on an XYZ orthogonal grid in XYZ space. The first necessary step was to interpolate the nodes on a regular grid (Figure 2b); then, to resample the surfaces to the scale required for modelling (25 m) (Figure 2c). From the original dataset of 177 irregularly spaced grid points for each surface, the final regular resampled grid contained 3363 x 3363 grid points. The 2048 x 2048 central block was taken forward for construction of the complete model.

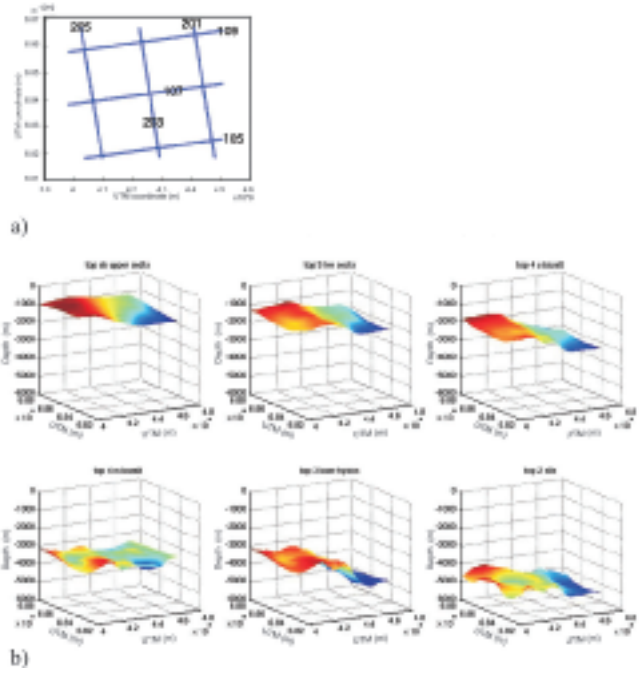

Figure 1 a) *GFA-99 campaign, grid of seismic lines; b) pre- and post-basalt sedimentary layers, top, mid and base basalt surfaces, as interpreted on the seismic data from the GFA-99 campaign at University of Durham. The data shown were interpreted at a 5 km node spacing.*

© 2005 EAGE

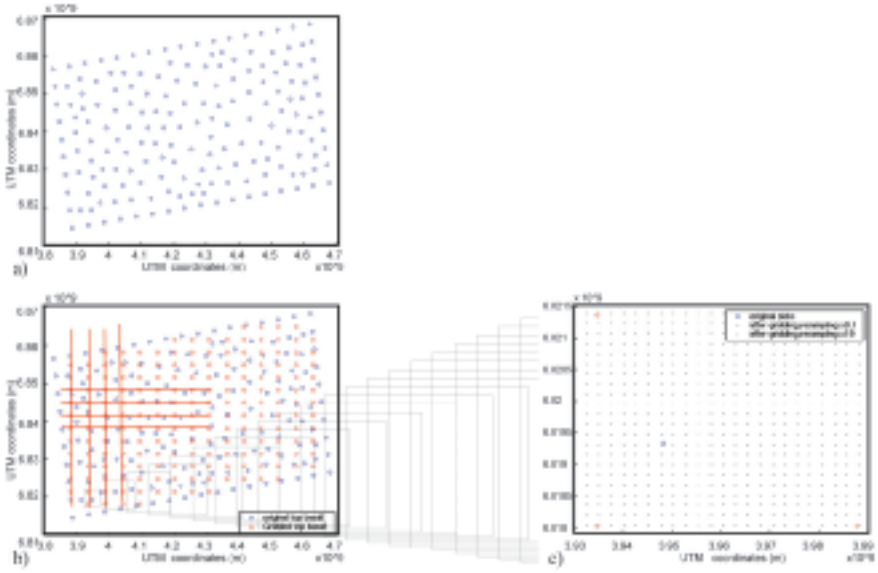

Figure 2 a) *Original top basalt interfaces picks, x and y positions. b) The picks are transformed to a regularly sampled grid, and then c) resampled to 25 m spacing. In c) zoom of a small area of the interface to see the new gridded points (black dots) that define the surface in relation to the gridded non-resampled points (red circles) and the original picks (blue circles).*

Fractal interpolation of the interfaces

Why?

Basalt interfaces, like most natural topographies (Mandelbrot 1977, Brown, 1985, Farr, 1992, Huang and Turcotte, 1989), have been shown to be fractal. Walia and Bull (1997), for example, established the fractality of basalt horizons in the southwest Rockall Plateau (NE Atlantic). The interfaces interpreted from seismic data resolve only the long wavelengths of the horizon roughness. The small-scale (controlled by the seismic wavelength used in acquisition) heterogeneity of the actual seismic reflectors cannot be resolved on the data. Hence, this information is missing on seismic sections. This can be observed in the amplitude spectrum of the image of the interface. The amplitude spectrum is given by the logarithm of amplitude plotted versus the logarithm of the spatial wavelength. The theoretical amplitude spectrum of an interface interpreted and digitized from seismic data is sketched in Figure 3. Information on medium to large-scale features is present (Figure 3, solid line); however, the amplitude information for the small-scale features is missing (Figure 3, dotted line). The fractal interpolation is used to restore these small-scale structures, in a statistical manner. The procedure is described in detail in the next section.

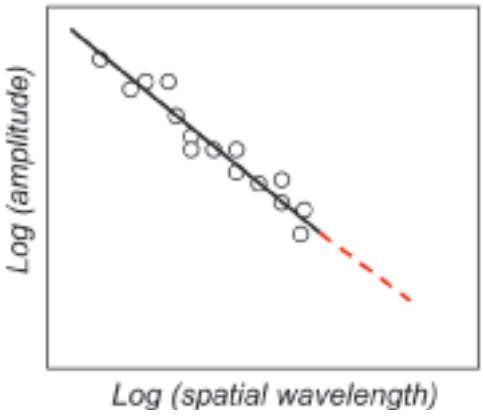

Figure 3 a) *Theoretical schematic amplitude spectrum of an interpreted seismic horizon. Information on medium to large-scale features is present (black dots), and on this we can measure the fractal dimension (from the slope of best fit line). However, the amplitude of the small-scale features is missing (red dotted line).*

Procedure

The log amplitudes of a fractal interface plotted versus log wavelength lie on a straight line, the slope of which relates to the fractal dimension of the interface. We can therefore extrapolate the values missing at the high frequencies and generate them synthetically. The lower spatial frequency information of the interface interpreted from seismic data are kept and merged with higher spatial frequency components derived from fractal surfaces generated synthetically with the same fractal dimension as measured on the digitized horizons. Hence we statistically create the missing small-scale features represented by the dotted line in Figure 3 (Walia and Bull, 1997).

In steps:

- The fractal dimension, mean amplitude value, and its standard deviation are estimated from the digitised interface;

© 2005 EAGE

- A fractal synthetic profile with the same fractal dimension and including low and high frequency components is generated;
- The high frequency components are extracted from this synthetic profile cut at the appropriate frequency to match the highest frequency in the real digitised data (using a Gaussian filter); and
- This high frequency component is added to the digitized interface.

Application to a synthetic profile is shown in Figure 4. The original signal is plotted in blue; the amplitude spectrum was calculated and the fractal dimension measured on it. A fractal synthetic profile was generated with the same fractal dimension, for higher frequency components (plotted in red). The high frequency component (in red) is added to the original signal (in blue), to obtain the final interpolated signal (plotted in green). Here we show the application to a profile, for simplicity of visualization. In case of surfaces, the fractal interpolation procedure applied is analogous.

Application

The procedure described in the previous section has been applied to the top basalt, mid series, and base basalt interfaces interpreted on the GFA-99 seismic data (Figure 1). However, for the real data, the simple procedure outlined above had to be modified because the geometry of the surfaces digitized from the seismic data contained a large contribution from post-depositional tectonic deformation and subsidence. So, to estimate the fractal dimension of the original basalt surface, these post-depositional effects were stripped off. This was achieved by subtracting from the basalt interfaces the geometry of the sedimentary layer immediately above (Figure 5). We refer to the result as the pre-tectonic deformation interface. While the fractal dimension was calculated on the pre-deformation interface, the standard deviation of the interface depth was calculated on what we refer to as the 'residual interface'. This is obtained by subtracting from the pre-tectonic deformation interface its best-fit line (Figure 6). If the standard deviation was calculated on the pre-deformation interface, the value would be unrealistically high, due to the slope of the

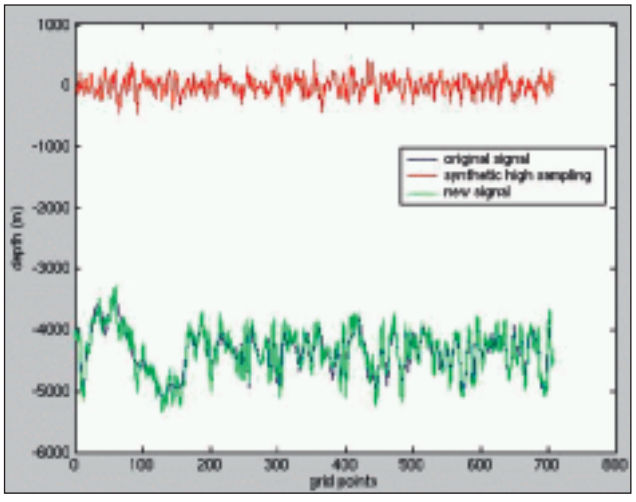

Figure 4 *Fractal interpolation applied to a synthetic profile: original synthetic signal in blue. Only the low frequency component is present. High frequency signal is synthetically generated (plotted in red) and added to the original signal. Result plotted in green.*

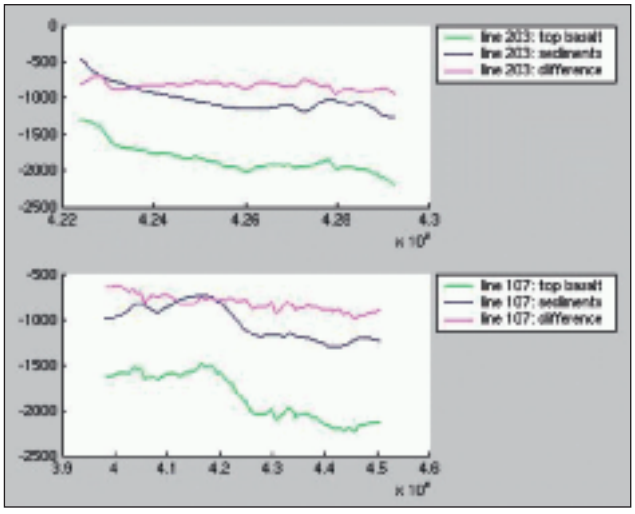

Figure 5 *Original top basalt interface profiles from line 203 and 107, in green. To the original profile (in green), the geometry of sediments above it (in blue) was subtracted in order to obtain the pre-tectonic (in magenta).*

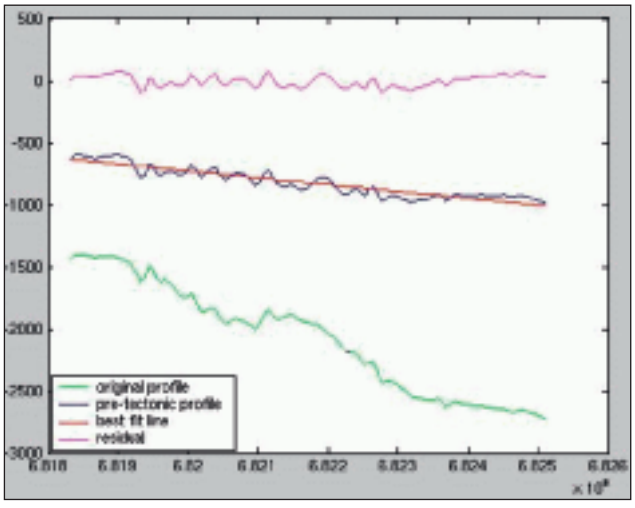

Figure 6 *Original top basalt interface profile from line 105 in green. To the original profile (in green), the geometry of sediments above it was subtracted in order to obtain the pre-tectonic deformation profile (in blue). On this, the best-fit line was calculated (in red) and subtracted to the pre-deformation profile to obtain what we refer as the 'residual' interface (in magenta). The standard deviation was calculated on the residual interface, while the fractal dimension on the pre-deformation interface.*

© 2005 EAGE

profile. Subsequently, the fractal interpolation procedure described above was applied to the data, and then the sediment geometry was added to recreate the basalt interface including the shorter wavelength features. The steps involved in this procedure are shown for one profile (GFA-99-203) in Figure 7.

In the amplitude spectrum of the resulting interface (Figure 7), the high frequency component that has been added is not a perfect continuation of the original data spectrum (Figure 7b, in cyan and blue). This is due to the fact that, as previously stated, the fractal dimension of the profile was calculated on the pre-deformation interface (Figure 7b, in black), while the standard deviation of the interface was calculated on 'residual' interface (Figure 7b, in magenta). The slope of the two segments of the amplitude spectrum is the same (the slope defines the fractal dimension) but the new segment of the spectrum fits only as a continuation of the 'residual' interface spectrum. Part of a profile extracted from the top basalt surface for Line 105 is shown before and after the application of fractal interpolation in Figure 8.

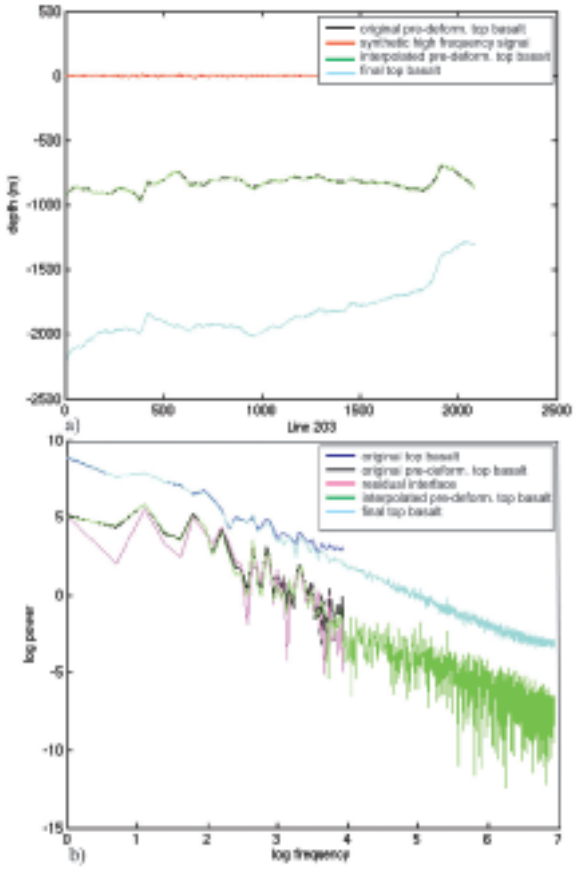

Figure 7 *Line 203, profile extracted from the top basalt surface shown at different stages of the fractal interpolation technique, as explained in the text. The spatial data are shown in (a) and the amplitude spectra for the same profile at different stages of the fractal interpolation procedure are shown in (b). Top basalt surface in blue; pre-deformation top basalt in black; the high frequency signal was generated (in red) and added to the pre-deformation top basalt (in black). In cyan the new interpolated top basalt interface. The sediments geometry was added back to obtain the final top basalt (green).*

Layers

Basalt thickness

Having defined the surfaces of the basalt body we still need to account for the internal heterogeneity. From geological observation and interpretation of the seismic data we identified that the basalt volume in the model region was filled with tabular flows, with a distinction between the upper basalt series, between the top and mid basalt interface, and a lower basalt series, between the mid and base basalt interface. The statistical values used to populate each flow in the upper basalt series were derived from an analysis of a large dataset of sonic logs taken from the Ocean Drilling Project (ODP) (Flood et al., 1995) and other wells through basalt layers. Tabular basalt flow was identified in several sonic logs on the basis of the geological description available in the log. The velocity values were statistically analyzed within the individual log; also the different logs were 'assembled' together and the statistical values extracted from those cumulative data. Both the individual log and the assembled log gave the same estimates for mean velocity, standard deviation of the velocity, and the fractal dimension (expressed

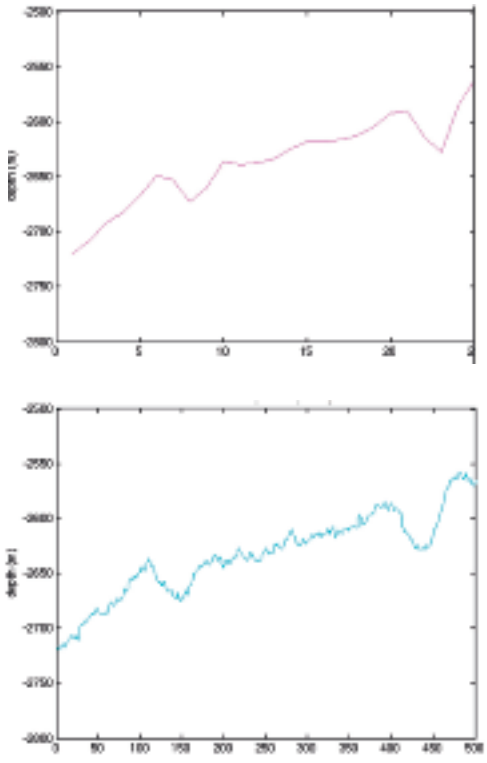

Figure 8 *Line 105, profile extracted from the top basalt surface, before (on the left, in magenta) and after (on the right, in cyan) the fractal interpolation technique.*

© 2005 EAGE

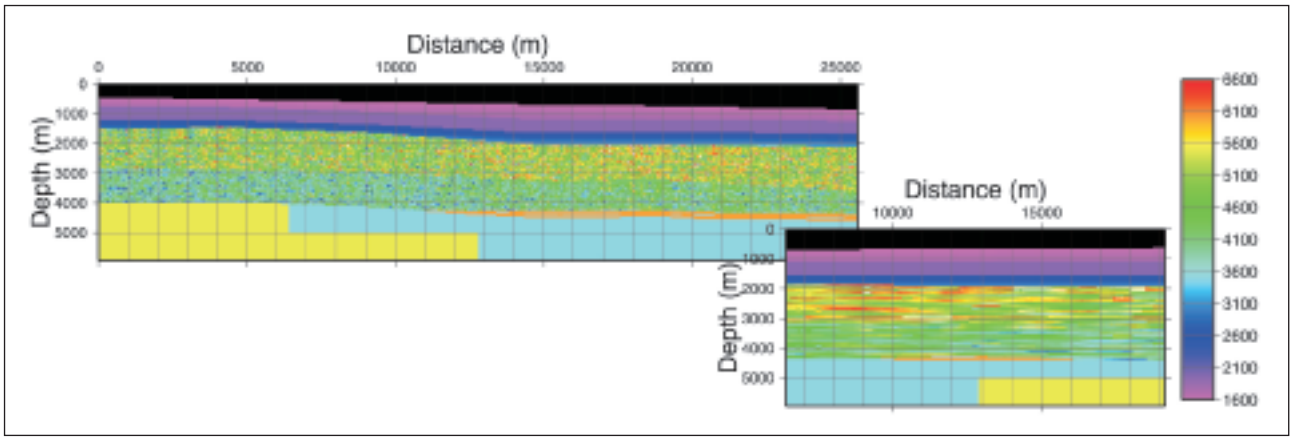

Figure 9 *Orthogonal vertical slices at the centre of the 3-D model, in the synthetic data survey area, along y=12800m, 1:1 scale.*

through the Hurst exponent H) of v_{mean}=4870 m/s, σ=680 m/s, H=0.3. Each layer is generated as a different realization of the same fractal medium. The correlation length in one horizontal direction is five times longer than in the other. This was done to add directional horizontal structural anisotropy. The correlation length in the vertical direction was chosen to be larger than eight grid points, which is the maximum thickness of a layer. Hence the correlation length is effectively infinite in the vertical direction. The average thickness of every flow, if the layers were tabular, is set to four grid points (100 m) and the flows are separated by fractal surfaces, defined by Hurst exponent H=0.7 (Walia and Bull, 1997) with a standard deviation of 8%. The grid node spacing of 25 m was chosen as a compromise between retaining sufficient fractal information, the expected run-time of the wave-propagation software (Wild et al., 2000) and the wavelength of the seismic source (~500 m) with a dominant frequency of 10 Hz. The flows created in this way were added to the pre-tectonic deformation basalt surfaces to fill the volume between the top and mid-basalt. From the seismic data the interpreted lower basalt series appeared as a less reflective volume. The geological explanation was that these probably represent basalts from less evolved magmas, with some hyaloclastites where the lava interacted with water. To fill this volume, a second realization of the basalt volume was created based on the upper layer but with the mean velocity reduced to 4090 m/s and the standard deviation reduced by 20%. Between the upper and lower basalt, a thin homogeneous layer was added in areas that were undefined to ensure a continuous basalt layer. The maximum thickness of the layer was 125 m and the velocity was set to 4200 m/s.

The velocity model was converted into density as follows:

$$\rho=1700+0.2*v$$

where ρ is density (gr/cm^3) and v the P wave velocity (m/s; Sheriff and Geldart, 1995). This conversion was initially tested on the sonic logs: the values obtained converting the sonic log into density show a good fit with the density log recorded in the same borehole. This relationship was used for the whole model. The S-wave velocity was set to 1/sqrt(3) of the P-wave velocity, and an intrinsic P-wave Q of 200 and an S-wave Q of 66 were included.

Above/below basalt

The remainder of the model was based on the geological model derived from an interpretation of the GFA-99 survey seismic data and inversion of satellite gravity data. This included:

- post-basalt sediment layers (as interpreted on seismic data);
- a thick sill at the base of the lower series (as interpreted on seismic data);
- a pre-basalt basin data; and deepening to the east.

The base sill has a serpentine-shaped edge and is present in the region of the model with the thickest sub-basalt sedimentary layer to the 'east' of the model. The basement strikes at 30° 'north', with the basalts lying directly on basement to the 'north west' and two faults that create a 2 km deep pre-basalt basin in the 'south east' (Figure 9). The interfaces of those layers were left as smooth as derived from the interpretation of the data, i.e. the fractal interpolation was not applied. A constant homogenous velocity was assigned to the sills (6000 m/s), the basement (5500 m/s), and the pre-basalt sediments (3500 m/s). The post-basalt sediments were divided into three layers. The upper and lower layers have a small velocity gradient of 50 m/s per 25 m depth below interface. The upper layer ranged from 1600 m/s to a maximum value of 1800 m/s, the middle layer is 800 m thick and has a constant velocity of 1950 m/s, and the lower layer ranged from 2300 m/s to maximum value of 3100 m/s. The density and S-wave velocity used the same relationships as used for the basalts but the P- and S-wave Q values were set to infinite.

The final model

The final model size of 2048 x 2048 x 180 grid points, at 25 m grid spacing gives a spatial dimension of 51.175 km x 51.175

© 2005 EAGE

km, and 4.475 km depth. The synthetic seismic data were acquired over a sub-volume of the model 25.6 km from west to east and 12.8 km from north to south. Slices from the volume are shown in Figure 10. The size of the final model was dictated by computer resources available for the simulation. The final 3D model has seismic characteristics very similar to the GFA-99 seismic data. Figure 11 shows a comparison between a phase screen (Wild et al., 2000) 2D exploding reflector section simulated on the final 3D model and a stack section from line GFA-99-107.

Acquisition and data

The model was used to generate seismic and non-seismic synthetic data, to test different processing routines and the integration of different methods for improving the sub-basalt image. Since the model is synthetic, the results can be compared with the original model to verify their accuracy.

Seismic data

3D seismic data have been generated on the model with an elastic phase screen simulator (Wild et al., 2000) on a 10 node pc cluster now based at the University of Durham. The 3D seismic dataset was created by repeatedly shooting a swath of 2D lines, simulating typical marine acquisition with eight streamers. The acquisition layout is shown in Figure 12: eight cables towed at 15 m below the sea-surface with a cross-line separation of 100 m, each with 240 channels spaced at 25 m. Shots were fired with a 200 m minimum offset. The source uses a wavelet recorded from a real airgun array towed at a depth of 10 m. Each swath records 320 shots per line, spaced at 50 m, with a sail line spacing of 400 m, to give a fully populated 3D grid with a cross-line bin width of 50 m and an inline bin width of 12.5 m. The data were simulated both without and with free-surface and internal multiples, to provide ideal shot gathers after perfect multiple and peg-leg removal and a more challenging dataset where the free-surface multiple and scattering dominates the later record.

Shot gathers recorded at the eight streamers for the shot at location x=13000m and y=12800, are shown in Figure 13 (a: without and b: with multiples) The key reflections for the shot gather marked in Figure 13 are labelled in Figure 14. For clarity, this shot gather does not include the free-surface multiples nor internal peg-legs. As the phase screen method gives a narrow-angle approximation, the wavefield is muted as it approaches critical angle, also wide-angle and refracted arrivals are suppressed and can be considered to be similar to field data after tau-p filtering to suppress energy travelling at

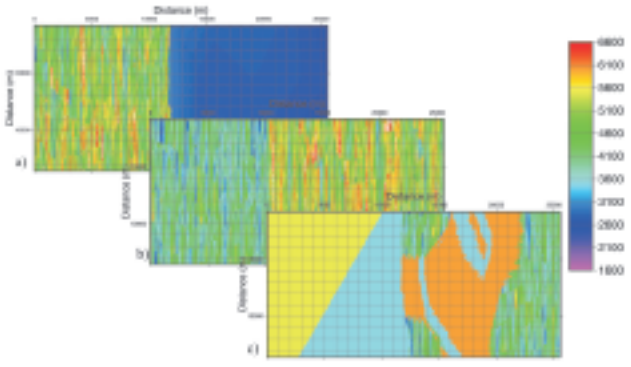

Figure 10 *Horizontal slices of the 3D model, at depth a) 1800 m, b) 3000 m and c) 4300 m, 1:1 scale.*

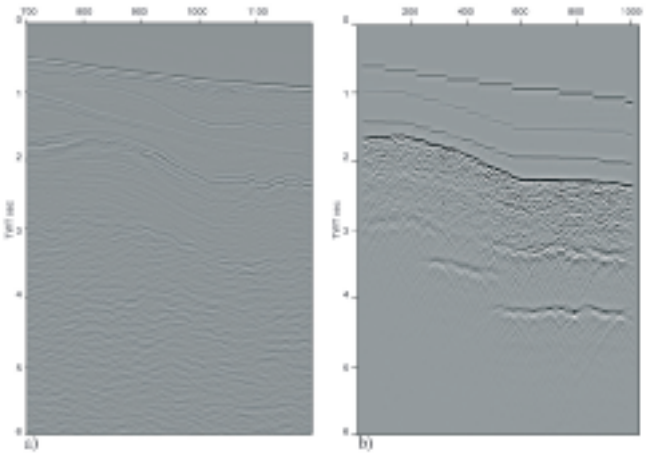

Figure 11 *Comparison between a) stack section from line GFA-99-107 and b) 2D exploding reflector section generated on the final model. The match in arrival times of the different events is very good.*

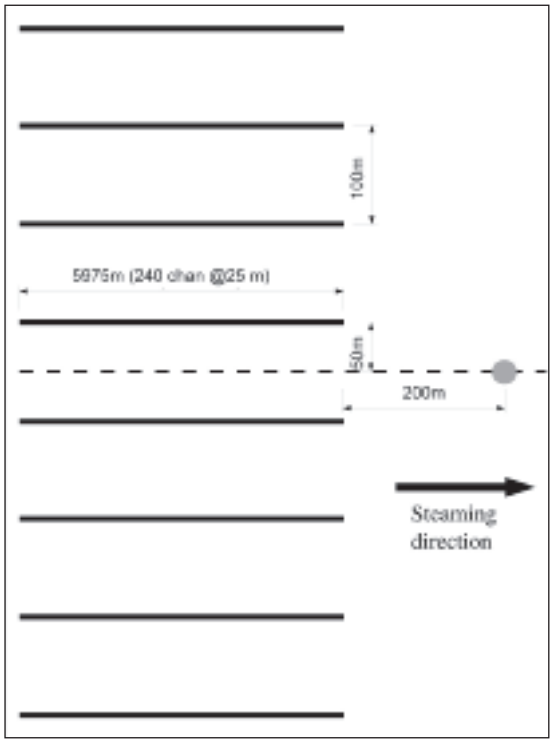

Figure 12 *Acquisition geometry for the synthetic data simulation.*

© 2005 EAGE

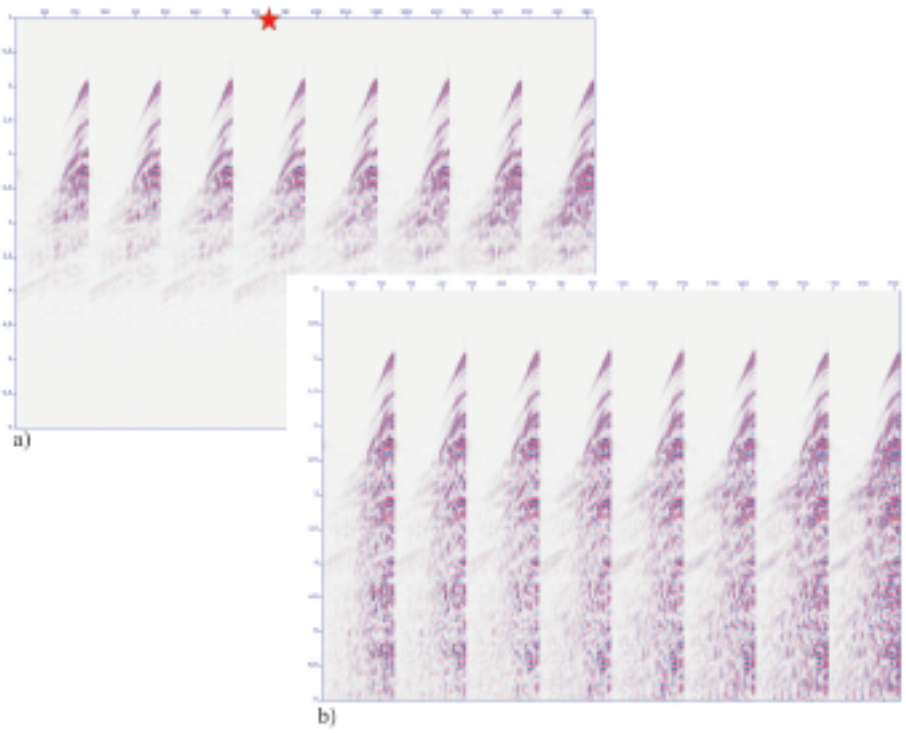

Figure 13 *Synthetic shot gathers recorded at the eight streamers for shot at location x=13000 m, y=12800 m, a) without multiples, b) with multiples. The star indicates the shot gather labelled in Figure 14.*

the lower velocities. The seabed and two sedimentary horizons give large amplitude hyperbolic shaped coherent arrivals; strong P- to S-wave conversions can be identified. The top basalt has large amplitude but the rough interface causes distortion in the expected arrival time; the amplitude of the arrival is suppressed at offsets greater than 1.5 km, because the combination of high velocity and basalt depth means that the critical angle is quickly reached at relatively short offsets. The internal reflectivity of the basalt is confused, with few coherent events. The P-wave basement reflection can be seen at all offsets and is the last strong coherent event seen on the gather. No evidence of a basement reflection from energy that has crossed the basalt as an S-wave can be seen. This is consistent with wave-propagation and scattering theory, that predicts that the lower velocity, shorter wavelength S-waves will be more strongly scattered in the basalt layer than the P-wave energy (see Martini and Bean. 2002a, for a specific sub-basalt imaging application). The data that include the free-surface and peg-leg energy show evidence of strong energy throughout the sub-basalt record. The fact that the energy is concentrated at the near offsets means that the multiple energy is dominated by reverberation in the layers above the basalt. The multiple of the basement reflection can be seen, which confirms that once the P-wave has passed through the basalt layer and the higher frequency energy has been stripped away, the residual wavelet can repeatedly pass through the basalt without further loosing its coherency.

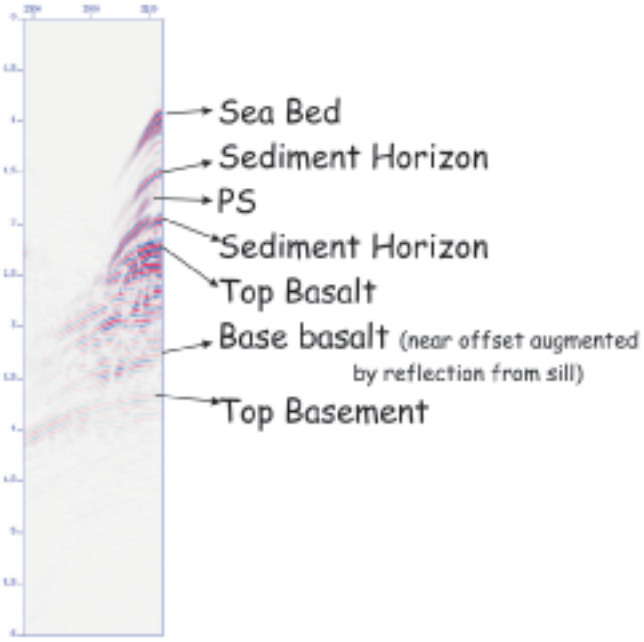

Figure 14 *Key reflections labelled on one of the raw shot gathers (marked by a star in Figure 13).*

Non-seismic data

Forward computation of the gravity and magnetic response of the 3D model has been performed, and it is shown in

© 2005 EAGE

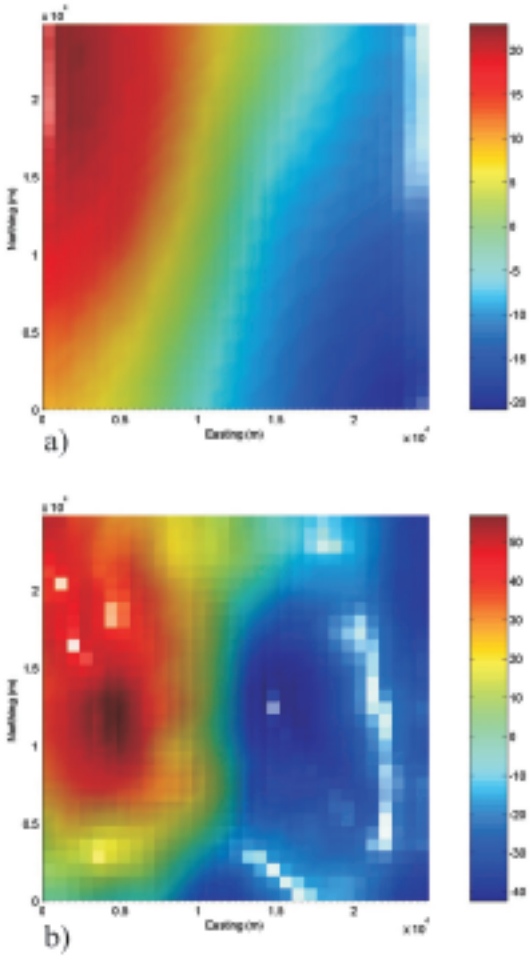

Figure 15 a) *gravity and b) magnetic synthetic response of the 3D model.*

Figure 15 a and b. The modelling was done by mapping the individual layers as 2D surfaces, then assigning a constant density and susceptibility to each layer (Table 1). The choice of assigning a constant value to each layer instead of parameterizing at the level of individual flows comes from the observation that the basalt is buried under a sediment cover: therefore we record the bulk effect while the high frequency variations caused by small-scale anomalies or thin bedding would not be observed. The magnetic model is based on the assumption that the basalt layers in this area are from the middle and upper series (Waagstein, 1988); these layers are reversely magnetized with only a weak remaining magnetization. This is consistent with the model by Smallwood et al., (2001) where the GFA-99 survey ties with the BIRPS-FAST line. The gravity shows the underlying basement trend of 30° north, whereas the magnetic data is more sensitive to the more north-south strike of the slope on the top basalt surface.

MT soundings were acquired on a 4.8 km grid over the whole 3D model. Resistivity values are given in Table 1. As done for magnetic, also for MT modelling the properties were modelled at the level of gross layering. Bedding could cause MT anisotropy, when a stack of resistive and conductive layers is present. Hence, primary and induced currents that flow parallel to the bedding would 'see' some average value for conductivity, whereas currents that are orthogonal to the bedding would 'see' an anomalously low conductance. MT measurements are dominated by horizontal currents, therefore are not affected by the effect of anisotropic layering (as for example controlled source EM would, for the strong vertical component of the currents). Azimuthal anisotropy would have a larger effect on MT data in the presence of significant lateral changes. For our basalt model, we have the same vertical layering, though the correlation length is different in the two directions. By implicitly assuming an isotropic layer, we have made the assumption that the connectivity of any fluids in the basalt is the same in both horizontal directions: we believe this assumption is valid, given that the vertical layered structure is the same. Testing showed that there was little 3D effect so each MT sounding is computed using a local 1-D approximation. Twenty frequencies were computed ranging from 1.86 Hz to $1x10^{-6}$ Hz to cover the frequency range typically used in the field. Figure 16 shows the MT sounding curves for two stations located at north-west and south-east corners of the model. The effect of the low resistivity sub-basalt sediments can be seen in the figure. The red curve (north-west) has the resistive basalt sitting directly on the basement, whereas the blue curve (south-east) has 2 km of sub-basalt sediments. The difference is particularly marked in the phase component.

Table 1 *Density, magnetic susceptibility and resistivity values assigned to the individual layers for gravity, magnetic and MT modelling.*

Boundary	Horizon Information	Mean Density (Kg/m^3)	Magnetic Susceptibility (nT)	Resistivity (Ohm m)
0	Water	1000	--	0.3
1	Top Sediments	1770	--	1
2	Middle Sediments	1880	--	1.2
3	Lower Middle Sediments	2180	--	1.9
4	Top Basalt	2650	0.03	17.7
5	Intermediate Basalt	2500	0.022	6.8
6	Lower Basalt	2520	0.025	5.7
7	Lower Sills	2700	0.03	67.9
8	Lower Sediments	2400	--	2.5
9	Basement	2700	0.01	80

© 2005 EAGE

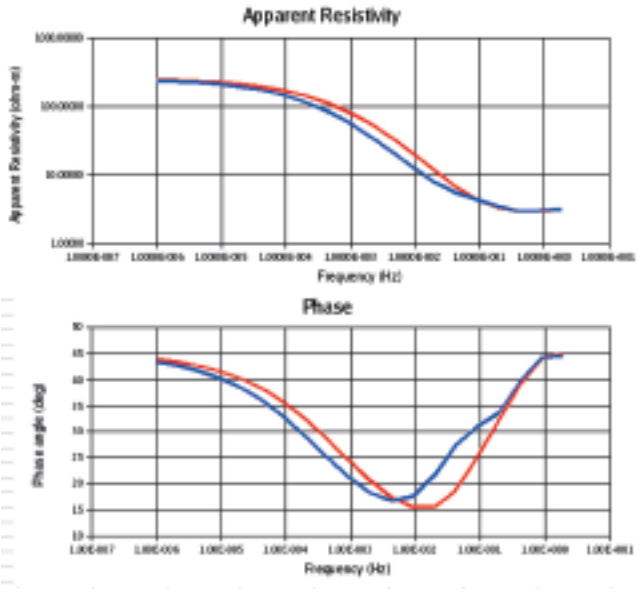

Figure 16 *Apparent resistivity response and phase for two locations on the model. The red curve is from a location with no sub-basalt sediments, whereas the blue curve is from a location with 2 km of sub-basalt sediments.*

Tests performed on 2D slices of the model suggested that the 1D approximation is acceptable for the model extent, though the will be some small error from inside the model. What has not been modelled is the effect due to the structure outside the model box, which could impose a large effect. While anyone using those results should be aware of this limitation, we believe that the simple progression of the MT anomaly from no sub-basalt sediment to 2 km of sub-basalt sediments demonstrated by this model is instructive for understanding the complex relationships in MT data.

Conclusions

A complex 3D model was built adapting all the information available from interpretation of seismic data, log data, gravity data, and geological observation. Seismic and non-seismic synthetic data have been produced on the model to be used in developing strategies for data integration into a common methodology to overcome the sub-basalt imaging problem.

The model and the data are available to the public, through the authors of the present paper.

Acknowledgements

The authors would like to thank D. Jerram in Durham University for stimulating discussions and useful insights into realistic geological models, ARK Geophysics for the model of the sub-basalt layers and the gravity and magnetic modelling, Marion Jegen for the MT modelling code, Anthony Mallon for compiling the rock property database, Paul Williamson and the anonymous reviewers for useful comments which helped to improve the manuscript. This work is sponsored by the SIMBA project, EU ref: ENK6-2000-00075.

References

Aminzadeh, F., Brac, J., and Kunz, T. [1997] 3-D Salt and Overthrust Models. *SEG/EAGE 3-D Modeling Series No.1*. Soc. Explor. Geophysicists, Tulsa.

Bagaini, C, Hansen, J.O., Kostov, C., and Ronen, S. [2000] Contributions of wide-angle P and PSP data to sub-basalt imaging. *Petex Conference, London. Expanded Abstract.*

Brown, S.R. and Scholz, C.H. [1985] Broad bandwidth study of the topography of natural surfaces. *J. Geophys. Res.* **90**, 12575-12582.

Crawford, W.C. [2002] Sub-basalt imaging using sea floor compliance: a case study. *J. Conf. Abstr.* 7, 2, 141.

Farr, T.G. [1992] Microtopographic evolution of lava flows at Cima volcanic field, Mojave desert, California. *J. Geophys. Res.* **97**, 15171-15179.

Fliedner, M.M. and White, R.S. [2001] Seismic structure of basalt flows from surface seismic data, borehole measurements and synthetic seismogram modelling. *Geophysics* **66**, 6, 1925-1936.

Flood, R.D., Piper, D.J.W., Klaus, A., et al. [1995] Proceedings of the Ocean Drilling Program, Initial Reports. College Station, TX, *Ocean Drilling Programme.*

Gibson, B. S. and Levander, A.R [1998] Modelling and processing of scattered waves in seismic reflection surveys. *Geophysics* **53**, 466-478.

Hautot, S., Perrot, J., Jegen, M.D., Cairns, G., and Tarits, P. [2002] Feasibility study of joint magnetotelluric/ seismic interpretation for sub-basalt imaging. *J. Conf. Abs.* 7, 2, 150-151.

Hestholm, S.O. and Ruud, B. [2000] 2D finite-difference viscoelastic wave modelling including surface topography. *Geophysical Prospecting*, **48**, 341-373.

Huang, J. and Turcotte, L. [1989] Fractal mapping of digitized images: application to the topography of Arizona and comparisons with synthetic images. *J. Geophys. Res.* **94**, 7491-7495.

Jerram, D. A. [2002] Vulcanology and facies architecture of flood basalts. *Volcanic Rifted Margins: Geological Society of America Special Paper*, **362**, 119-132.

Jegen, M., Hautot, S., Cairns, G., and Tarits, P. [2002] Using electromagnetics to image sub-basalt sediments. *J. Conf. Abs.* 7, 2, 154-155.

MacGregor, L., Sinha, M., and Constable, S. [1999] Use of marine controlled source electromagnetic sounding for sub-basalt exploration. *61st European Association of Geoscientists and Engineers Conference and Exhibition, Expanded Abstract.*

MacGregor, L. and Sinha, M. [2002] Sub-basalt imaging using marine controlled source electromagnetic sounding. *J. Conf. Abs.* 7, 2, 172-173.

Mandelbrot, B.B. [1977] Fractals: Form, Chance and Dimension. *Freeman and Co., USA.*

Manglik, A. and Verma, S.K. [1998] Delineation of sediments below flood basalts by joint inversion of seismic and magnetotelluric data. *Geophys. Res. Lett.* **25**, 21, 4015-4018.

© 2005 EAGE

Martini, F. and Bean, C.J. [2002a] Application of pre-stack wave equation datuming to remove interface scattering in sub-basalt imaging. *First Break* **20**, 6 395-403.
Martini, F. and Bean, C.J. [2002b] Interface scattering versus body scattering in sub-basalt imaging and application of prestack wave equation datuming. *Geophysics* **67**, 5, 1593-1601.
Martini, F., Bean, C.J., Dolan, S.S., and Marsan, D. [2001] Seismic image quality beneath strongly scattering structures and implications for lower crustal imaging: numerical simulations. *Geophys. J. Int.* **145**, 423-435.
Martini, F., Hobbs, R.W. Bean, C.J., and Pandolfi, D., Seismic wave attenuation in basaltic rocks from VSP synthetic and real data. Submitted to *Geophysical Prospecting*.
Murphy, C., Mumaw, G.R., and Stalin, F. [2002] Resolving basalt and sub-basalt geology with high precision high resolution gravity gradient data. *J. Conf. Abs.* **7**, 2, 178-179.
Paul, A. and Campillo, M. [1988] Diffraction and conversion of elastic waves at a corrugated interface. *Geophysics* **53**, 1415-1424.
Pullammanappallil, S., Levander, A., and Larkin, S.P. [1997] Estimation of crustal stochastic parameters from seismic exploration data. *J. Geophys. Res.* **102**, 15269-15286.
Purnell, G.W., Hampson, G., and McDonald, J.A. [1990] Effects of interface roughness on wave propagation. *60th Meeting, Society of Exploration Geophysicist, Expanded Abstract.*
Ruud, B. and Hestholm, S. [2000] 2-D surface topography boundary conditions in seismic wave modelling. *70th Meeting, Society of Exploration Geophysicists, Expanded Abstract.*
Sheriff, R.E. and Geldart, L.P. [1995] *Exploration Seismology.* Cambridge University Press.
Single, R.T. and Jerram, D. A. [2004] The 3D facies architecture of flood basalt provinces and their internal heterogeneity: examples from the Palaeogene Skye Lava Field. *Journal of the Geological Society*, **161**, 911-926.
Smallwood, J.R., Towns, M.J., and White R.S. [2001] The structure of the Faeroe-Shetland Trough from integrated deep seismic and potential field modelling. *Journal of the Geol. Soc. London* **158**, 409-412.
Versteeg, R. [1994] The Marmousi experience: Velocity model determination on a synthetic complex data set. *The Leading Edge* **13**, 927-936.
Waagstein R. [1988] Structure, composition and age of the Faeroe basalt plateau. In: Early Tertiary Volcanism and the Opening of the NE Atlantic (eds A.C. Morton and L.M. Parson), 225-238. *Special Publication 39, Geological Society, London.*
Walia, R.K. and Bull, J.M. [1997] Modelling rough interfaces on seismic reflection profiles-the application of fractal concepts. *Geophys. Res. Lett.* **24**, 16, 2067-2070.
Warren, R.K. and Srnka, L.J. [1992] Exploration in the basalt-covered areas of the Columbia River Basin, Washington, using electromagnetic array profiling (EMAP). *Geophysics* **57**, 8, 986-993.
Wild, A.J., Hobbs, R.W., and Frenje, L. [2000] Modelling complex media: an introduction to the phase screen method. *Phys. Earth Plan. Int.* **120**, 219-225.
Ziolkowski, A., Hanssen, P., Gatliff, R., Jakubowicz, H., Dobson, A., Hampson, G., Li, X-Y., and Liu, E., [2003] Use of low frequencies for sub-basalt imaging. *Geophysical Prospecting* **51**, 169-182.

© 2005 EAGE